2*s* photoionization and subsequent Auger cascade in atomic Si

L. Partanen,[1,*] S. Fritzsche,[1] K. Jänkälä,[1] M. Huttula,[1] S. Urpelainen,[1,2] S. Osmekhin,[1] H. Aksela,[1] and S. Aksela[1]

[1]*Department of Physics, University of Oulu, P. O. Box 3000, 90014 University of Oulu, Finland*

[2]*MAX-lab, Lund University, P. O. Box 118, SE-22100 Lund, Sweden*

(Received 26 April 2010; published 28 June 2010)

The 2*s* photoionization and subsequent Auger transition cascade in atomic Si were studied by means of synchrotron-radiation-induced electron spectroscopy. After the 2*s* photoionization, the core hole states decay predominantly by a two-step Auger transition cascade into the triply ionized [Ne]*nl* states. The ionization channels of the 2*s* core-ionized Si^+ atoms to Si^{3+} ions were observed by measuring the conventional Auger electron spectra of the L_1-$L_{2,3}M$ Coster-Kronig transitions and the $L_{2,3}M$-*MMM* Auger transitions. The observed L_1-$L_{2,3}M$ and $L_{2,3}M$-*MMM* Auger spectra were analyzed by means of extensive multiconfiguration Dirac-Fock computations. We found that the electron correlation plays a prominent role in the Auger cascade, especially for the final-step Auger $L_{2,3}M$-*MMM* spectrum. Additionally, it was seen that the $L_{2,3}M$-*MMM* Auger spectrum of Si includes more Auger groups than the isoelectronic $L_{2,3}$-*MM* Auger spectrum of Al. Thus, more information on the intermediate ionic states is obtained if they are produced by Auger cascade rather than by direct photoionization.

DOI: 10.1103/PhysRevA.81.062513 PACS number(s): 32.10.−f, 32.80.Fb, 32.80.Hd, 31.15.A−

I. INTRODUCTION

The Auger transition cascade in atoms is a deexcitation process of several consecutive Auger decays. The initial state of the Auger transition cascade is created by a core-shell ionization. The Auger transition is called a Coster-Kronig transition if the initial vacancy is filled by an electron from a higher subshell of the same shell. Coster-Kronig transitions have a high decay probability, causing a broad lifetime width of the initial core state. Coster-Kronig transitions are followed by subsequent Auger transitions with the result that an atom goes through several intermediate ionic states. Of course, the same ionic states are created also via direct double- or multiple-ionization processes. At the end of the Auger transition cascade, the multiply charged ion is in a state that may further decay only radiatively.

According to the electric-dipole approximation, the total parity of the system changes in a photoionization process. This requires a change of $\Delta l = \pm 1$ of a single electron's angular momentum in the system. In the cases of normal photoionization and monopole shake-up transitions, the change of the angular momentum occurs for the continuum electron. On the other hand, the continuum electron may preserve its angular momentum and the change occur in a bound electron; this is referred to as a conjugate shake-up transition. Conjugate shake transitions are, however, usually weak compared to normal photoionization transitions (see, e.g., [1]). In an Auger decay, in contrast, the orbital angular momentum of the continuum electron is determined by the rule stating that the parities of the initial and final states must be the same.

In this work, we have studied the Auger transition cascade following a 2*s* photoionization of atomic silicon. The direct photoionization populates eight even-parity ionic states coupled from the $1s^2 2s 2p^6 3s^2 3p^2$ configuration, and *p*-type continuum photoelectrons are emitted. The 2*s* ionized states decay very rapidly by a subsequent Coster-Kronig (CK) transition to the Si^{2+} $1s^2 2s^2 2p^5 3s^2 3p(+\varepsilon s, \varepsilon d)$ even-parity ionic states or to the Si^{2+} $1s^2 2s^2 2p^5 3s 3p^2(+\varepsilon p, \varepsilon f)$ odd-parity ionic states, giving rise to a broad natural linewidth for both the 2*s* photolines and the CK lines. Because of a $2p$ ionized vacancy, further second-step Auger transitions take place and lead to a triply ionized atom with Si^{3+} [Ne]*nl* final states. In Fig. 1, we schematically display the level energies for different ionization states of Si and indicate by arrows the initial excitation and subsequent Auger transitions that have been observed in this work.

This study complements our previous studies of atomic Si and Al [2–4] in which the *L*-shell photoionization and subsequent Auger decay were studied. The 2*s* photoelectron and subsequent L_1-$L_{2,3}M$ CK and $L_{2,3}M$-*MMM* Auger spectra of atomic Si are studied here both experimentally and theoretically. The $L_{2,3}M$-*MMM* spectrum overlaps in kinetic energies with the $L_{2,3}$-*MM* Auger electron spectrum. To resolve the $L_{2,3}M$-*MMM* lines from the $L_{2,3}$-*MM* lines, the electron spectrum was measured with two photon energies, below and above the 2*s* ionization threshold. The satellite Auger lines originating from the direct photo double ionization of the $2p^5(3s,3p)^3$ states appear in both spectra. As will be shown, the satellite lines also receive intensity via the L_1-$L_{2,3}M$ CK channel. The L_1-*MM* Auger transition spectrum is about 55 eV above the $L_{2,3}$-*MM* Auger spectrum in kinetic energy. However, the L_1-*MM* transitions are assumed to be very weak, and they are excluded in this study. To explore the 2*s* photoelectron spectrum and its subsequent Auger cascades, multi-configuration Dirac-Fock (MCDF) calculations have been carried out for the L_1-$L_{2,3}M$ and $L_{2,3}M$-*MMM* spectra. The electron correlations are found to be important for the interpretation of the second-step $L_{2,3}M$-*MMM* Auger transitions where, apart from a $2p$ hole state, an additional hole within the *M* shell is involved. A similar strong effect of $2p$ hole states owing to electron-electron correlations has been previously seen in the $L_{2,3}$-*MM* transitions of atomic Al [3] and Si [4] atoms.

*leena.partanen@oulu.fi

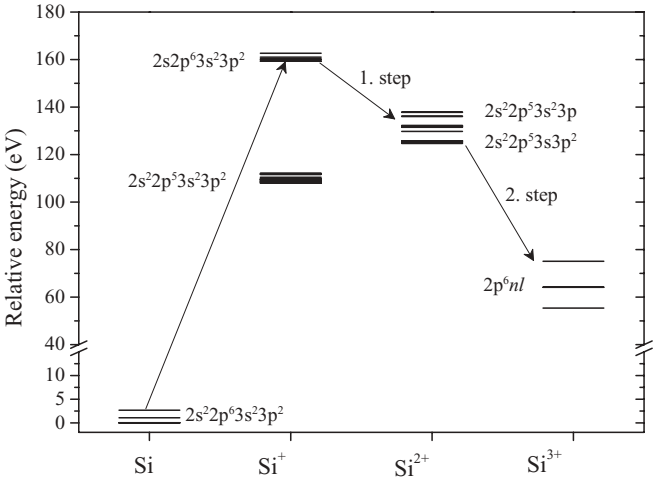

FIG. 1. Schematic electron energy levels of studied transitions.

II. EXPERIMENTS

The 2*s* photoelectron and subsequent CK and Auger electron spectra were measured at the I411 beamline of the MAX II synchrotron storage ring at Lund, Sweden. A modified Scienta SES-100 electron energy analyzer [5] was mounted at the angle of 54.7° with respect to the electric-field vector of the synchrotron radiation in order to achieve angle-independent intensity distribution in the recorded spectra. An effusive beam of Si atoms was produced with an inductively heated oven at the crucible temperature of about 1500°C. A detailed description of the oven system is given in Ref. [2]. As can be seen in Fig. 2, the natural linewidths of the 2*s* photoelectron and subsequent CK structures are very broad. So a fixed pass energy of 20 eV was used in measurements, providing a total experimental resolution of about 120 meV for the photolines. The spectra were measured with two different photon energies, 208 and 213 eV. This enabled us to reliably resolve the photoelectron lines from the Auger electron lines. The measured spectrum with the photon energy of 208 eV is depicted in Fig. 2. The kinetic energies of the photoelectron and L_1-$L_{2,3}M$ CK spectra were calibrated with the aid of the $L_{2,3}$-*MM* Auger lines of Si from Ref. [4] located in the kinetic energy region of 50–60 eV. The pure $L_{2,3}$-*MM* spectrum measured with the photon energy of 135 eV (published in Ref. [4]) was subtracted from the 2*s* photoelectron and L_1-$L_{2,3}M$ Auger spectrum shown in Fig. 2.

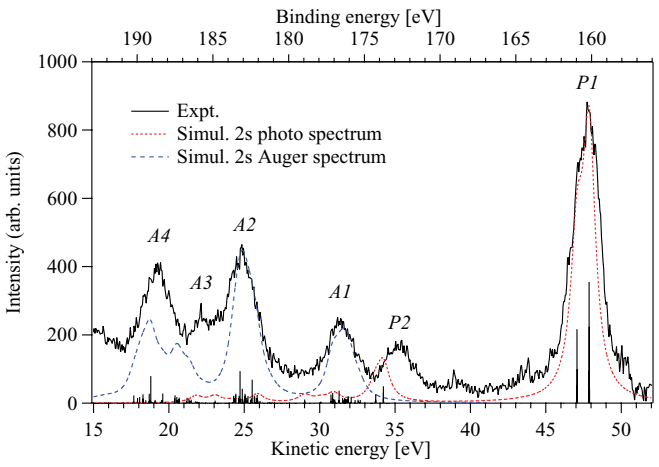

FIG. 2. (Color online) 2*s* photoelectron structures *P*1 and *P*2 and subsequent Coster-Kronig transition groups *A*1–*A*4. The experimental spectrum (solid line) was measured with the photon energy of 208 eV. Top axis gives the binding energies for the photoelectron lines (dashed line). The simulated Coster-Kronig groups (dotted line) were shifted 2.8 eV toward low kinetic energies. The 2*p* Auger structure is subtracted from measured spectrum.

The $L_{2,3}M$-*MMM* Auger lines in the kinetic energy region 50–80 eV with very narrow natural widths were recorded with high-resolution settings using an analyzer pass energy of 5 eV. In order to attain a reasonable count rate, the synchrotron radiation was not monochromatized. Instead, the spectrum was measured using two different undulator gaps chosen so that the peak of the undulator first harmonic was located at the desired photon energy. The first photon energy was set to 135 eV, which is below the 2*s* ionization threshold of about 160 eV but above the 2*p* double-ionization threshold of about 125 eV. The second photon energy was chosen to be 200 eV, which is well above the 2*s* ionization threshold. Both $L_{2,3}M$-*MMM* Auger spectra are depicted in Fig. 3.

III. CALCULATIONS

For computations of the photoionization and Auger (cascade) spectra, the MCDF method was used to calculate the wave functions of the various steps and, hence, to derive the cross sections and relative intensities. In this method [6], all the atomic state functions of interest are approximated by linear combinations of symmetry-adapted functions, so-called configuration state functions (CSFs). This method has been utilized in a large number of case studies [6]. In the computations below, we have used the wave functions from the well-known GRASP92 code [7]. The necessary cross sections and rates were calculated by use of the RATIP package [8,9]. In particular, we made use of the PHOTO component [1,10] to account for the nonorthogonality of the radial wave functions in the computation of the photoionization lines for the initial hole states, which appeared to be very sensitive to the relaxation of the electron density after the removal of a 2*s* electron.

In the photoionization of inner-shell electrons, it is typically well justified to describe the initial ionization and the subsequent Auger emissions as individual steps of a common process. In the course of a cascade process, resonance states are created consecutively that are all embedded energetically within the continuum of the next-higher-charge state of the ion and, hence, will autoionize until a (nearby) stable state is reached. In such a cascade of included states, at least the resonance intermediate states are highly correlated (many-electron) states that are strongly affected by electron correlations, especially if inner-shell electrons or several open shells are involved in the computations

The two components of the RATIP program PHOTO and AUGER are built on a recently developed code for deriving the angular coefficients for various one- and two-particle operators [11] which have been utilized to obtain all the amplitudes due to the coupling of the bound-state electrons to

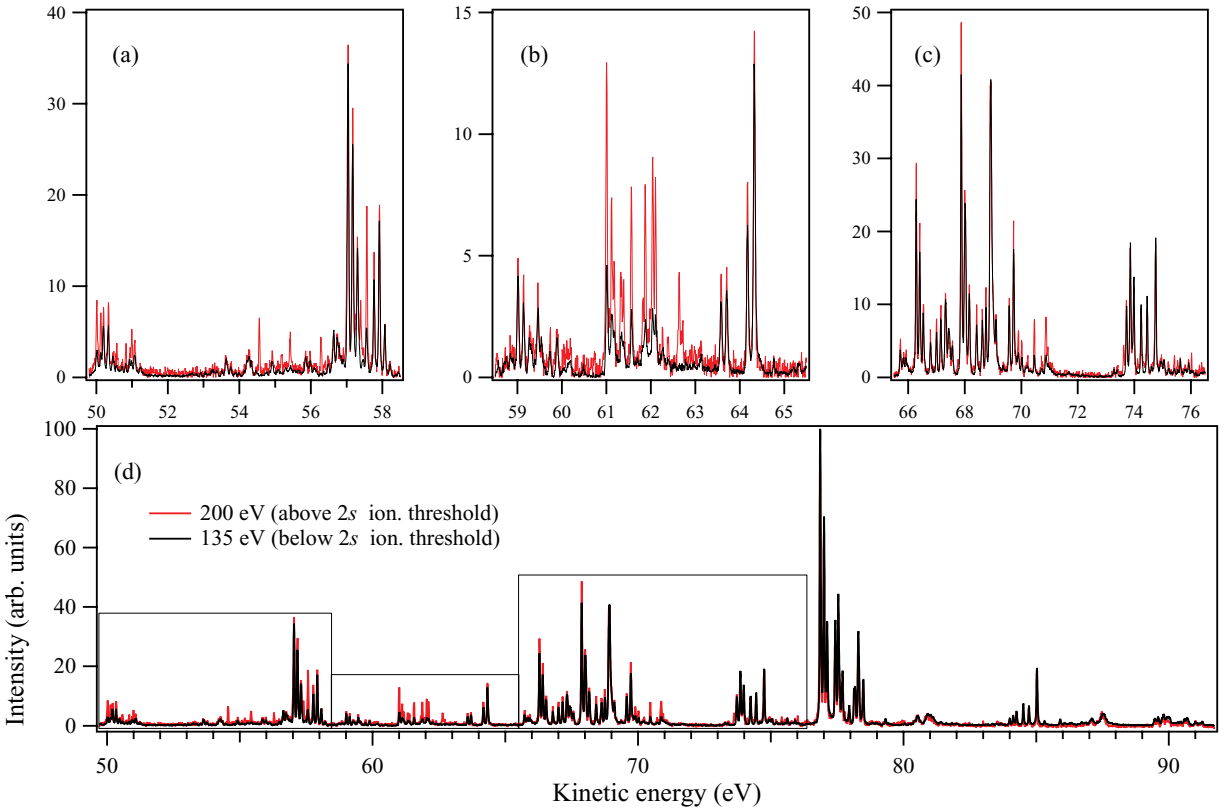

FIG. 3. (Color online) (a)-(c) Parts of the $L_{2,3}$-*MM* Auger spectrum of atomic Si which reveal the $L_{2,3}M$-*MMM* Auger satellite structure following from the 2*s* photoionization. (d) $L_{2,3}$-*MM* Auger spectrum measured with two undulator settings with the first-harmonic photon energy peak set in 135 (black line) and 200 eV (grey line).

the electron continuum. In these components, the (continuum) spinors of the emitted electrons are solved within a spherical but level-dependent potential of the final ion. This scheme includes both the direct and exchange interactions of the emitted electron with the bound-state density. While the full relaxation of the density was taken into account for the initial 2*s* ionization, it has been included only approximately for the subsequent electron emission because of the rapid increase in the number of scattering states that need to be included, and the fact that the Auger decay is caused by electron-electron correlations. The particular configurations that were used in the generation of the wave functions will be given in Sec. IV, where we explain, in turn, the individual steps of the cascades and their effects on the observed spectra.

As Si is a light atom, the electronic states of Si atom follow rather *LSJ* coupling than the *jjJ* coupling scheme. The transformation from *jjJ* to *LSJ* term notations was utilized using the code described in Ref. [12]. Only the *LSJ* notations are discussed here.

IV. RESULTS AND DISCUSSION

A. 2*s* photoelectron spectrum

The 2*s* photoelectron spectrum consists of two broad structures, labeled as *P*1 and *P*2 in Fig. 2, having the binding energies of 160 and 173 eV (obtained at the intensity-weighted center of each peak). The natural linewidth was determined to be about 1.2 eV and the same value was predicted by the calculations. The large linewidth results from the fast CK decay of the 2*s* ionized states, as discussed earlier. The binding energies for the individual $2s^{-1}$ states are impossible to determine because of the broad linewidths, but the most intense photolines are located in the binding energy region of 159.5–161.0 eV. In order to simulate the photoelectron spectrum, the dipole transitions from the ground configuration $1s^2 2s^2 2p^6 3s^2 3p^2$ states to the $1s^2 2s 2p^6 3s^2 3p^2$ ionic states were calculated. The satellite contribution was estimated with a multiconfiguration calculation, which was performed by including the states from the $2s2p^6(3s^2 3p^2 + 3s^2 3p4p + 3s3p^2 3d + 3s3p^2 4s)$ configurations. The Boltzmann distribution of the thermally excited $[\mathrm{Ne}]3s^2 3p^2(^3P_{0,1,2})$ ground configuration states was used, giving relative populations of 13%, 35%, and 52%, respectively. The weakly populated $3p^2(^1D_2)$ and $3p^2(^1S_0)$ states were not taken into account. In order to properly include the relaxation of the electron density caused by a 2*s* hole, independent MCDF computations were carried out for the initial and final states. The simulated spectrum is compared to the experimental one in Fig. 2. A Voigt line profile was used in the simulation with a Lorentzian linewidth contribution of 1.2 eV and a Gaussian contribution of 0.12 eV.

The calculations were found to reproduce well the energies and relative intensities of the structures *P*1 and *P*2. By making use of these simulations, the origin of the photoelectron peaks *P*1 and *P*2 can be identified. The intense structure *P*1 consists of two line groups (separated by 1 eV) that arise

from the transitions to the high- and low-spin fine-structure states of the $2s2p^63s^23p^2\,(^3P)\,^4P_J$ $(J = 1/2,3/2,5/2)$ and $2s2p^63s^23p^2\,(^3P)\,^2P_J$ $(J = 1/2,3/2)$ manifolds, as the five lowest states with a $2s$ hole. Thus, the $2s$ photoionization does not change the (^3P) parent term of the coupled $3p^2$ valence electrons. These $2s$ ionized states are very pure in the *LSJ* coupling scheme, as the average contribution of the dominant term in the atomic state function is about 0.96. Nevertheless, there is a minor contribution of about 0.02 of the $2s2p^63s3p^23d$ configuration states, which are found to be crucial in understanding the following Auger cascade.

The photoelectron structure *P*2 originates from the corresponding $3p^2 \rightarrow 3p4p$ shake-up transitions during the $2s$ photoionization. The *P*2 structure consists also of two high- and low-spin line groups originating from the transitions to the $2s2p^63s^23p4p\,^2P$ and $2s2p^63s^23p4p\,^4P$ states. The experimental shake-up probability was found to be about 17% of the main transitions while the calculated shake-up probability is about 12%. In addition, the calculations predicted intensity for several satellite states with an open $3s$ shell appearing below the shake-up satellites. Since the configuration interaction was found to be negligible, the strength of these lines indicates a strong orbital relaxation because of removal of a $2s$ electron.

B. L_1-$L_{2,3}M$ CK spectrum

The L_1-$L_{2,3}M$ CK spectrum consists of four separate line groups labeled as *A*1–*A*4 in Fig. 2. The same broad linewidths of 1.2 eV for the $2s$ photoelectron lines affect the L_1-$L_{2,3}M$ CK lines also. For this reason, the individual lines of the rich fine structure of the L_1-$L_{2,3}M$ Auger spectrum, marked with vertical lines in Fig. 2, cannot be resolved. Nevertheless, in order to simulate this spectrum, the Auger transition energies and probabilities from the most intense $2s$ ionized initial states were calculated. Since the major population of the $2s$ ionized states was distributed between the five lowest $2s2p^63s^23p^2$ states, we chose to do a full calculation of the Auger cascade only for these initial states. In order to take the valence electron correlation into account, the $2s$ ionized states were recalculated using the configurations $2s2p^6(3s^23p^2 + 3s^23d^2 + 3s3p^23d + 3p^4 + 3p^23d^2 + 3d^4)$ where the satellite configurations were omitted. These MCDF wave functions were used as initial states of the L_1-$L_{2,3}M$ CK transition calculations. The MCDF wave function calculations for the doubly ionized $L_{2,3}M$ final states were performed by including the $2s^22p^5(3s^23p + 3s3p3d + 3p^3 + 3p3d^2)$ configurations for even-parity states and the $2s^22p^5(3s^23d + 3s3p^2 + 3s3d^2 + 3p^23d + 3d^3)$ for odd-parity states. Relative intensities for the CK lines were obtained by distribution of the calculated population of the photoionized initial states between the final states in proportion to the Auger transition rates.

The shape and intensity of the CK line groups *A*1–*A*4 are predicted by calculations quite well, as can be seen from Fig. 2, even if the line group *A*3 is shifted toward higher kinetic energies, forming almost a shoulder of the peak structure *A*4. This shift is caused by electron correlation effects, and the Auger structures *A*2–*A*4 were found to be sensitive to the configuration basis used in the calculations. The calculated kinetic energies of the CK lines are higher than the observed one (i.e., the simulated spectrum was shifted for Fig. 2). The rather large shift of about 2.8 eV between experiment and theory can be explained by the strong CK coupling of the $2s$ hole states to the autoionization continuum, which modifies not only the widths of these resonance states but also their energy position [14]. The electron configurations involved in the L_1-$L_{2,3}M$ transitions could be assigned successfully to Auger groups *A*1–*A*4. The assignment between the observed energies and experimental and theoretical group intensities are given in Table I. In particular, the Auger group *A*1, which is well separated from the other line groups, arises from transitions to the even-parity $1s^22s^22p^53s^23p$ states. The Auger groups *A*2–*A*4 originate from the transitions to the odd-parity energy states having dominant $1s^22s^22p^53s3p^2$ character. The dominant state terms of the most intense transitions for the Auger groups *A*2 and *A*4 are also given in Table I. The Auger groups *A*2–*A*4 are characterized by the orbital angular momentum obtained from the $3p$-$3p$ coupled parent term as well as a rather strong spin-orbit interaction of the $2p^5$-$3s$ coupled states giving intensity to the *A*2 and *A*4 groups.

The $2s$ ionized states are almost pure in the *LS* coupling scheme. The effect of electron correlation, especially the configuration interaction between the Si^+ $2s2p^63s^23p^2$ and $2s2p^63s3p^23d$ configurations, is not evident in the L_1-$L_{2,3}M$ Auger spectrum, and single-configuration calculations predict quite well the broad structures of the L_1-$L_{2,3}M$ Auger groups. However, even a small contribution of other configuration states in the eigenvector may be significant during the subsequent Auger decay (see, e.g., [13]). As will be shown below, prominent Auger amplitudes between CSFs with a $3d$ electron produce strong Auger lines during the subsequent $L_{2,3}M$-MMM decay. Thus, the configurations with the occupied $3d$

TABLE I. Kinetic energies and relative intensities of L_1-$L_{2,3}M$ CK transitions. Initial and final configurations as well as theoretical values were obtained by MCDF calculations. The transitions originate mainly from the $2s2p^63s^23p^{2\,4}P,^2P$ initial states.

			Relative intensity (%)	
Label	Final configuration	Energy (eV)	Expt.	Theory
*A*1	$2p^53s^23p$	31.5	48	31
*A*2	$2p^53s(^1P)3p^2(^3P)[^3D_{1,2,3},^3P_2]$	24.9	100	100
*A*3	$2p^53s(^{1,3}P)3p^2(^1D)$	22.3	29	28
*A*4	$2p^53s(^3\mathrm{P})3p^2(^3P)[^3D_{1,2,3},^3S_1]$	19.4	85	53

orbital need to be included in the wave function expansion for the L_1 and $L_{2,3}M$ states.

C. $L_{2,3}M$-MMM Auger spectrum

The binding energies of the Si^{2+} $2p^5 3s^2 3p$ states are above the Si^{3+} ionization threshold at 58.0 eV [15]. Thus, the Si^{2+} states can further decay via subsequent $L_{2,3}M$-MMM Auger transitions. The $L_{2,3}M$-MMM Auger lines are located as satellite structures in the same kinetic energy region as the normal $L_{2,3}$-MM Auger lines populated by the direct $2p$ ionization. It is quite a challenge to separate this much weaker Auger spectrum from the strong $L_{2,3}$-MM lines. Moreover, additional contributions to these peaks may arise also from Auger decay following photo double ionization. By measuring the spectrum with two different photon energies above and below the $2s$ photoionization threshold, the $L_{2,3}M$-MMM Auger lines can be separated from the $L_{2,3}$-MM Auger lines because of the increase of the $L_{2,3}M$-MMM intensity. As seen in Fig. 3, some lines become more intense when the $2s$ photoionization channel is possible. These $L_{2,3}M$-MMM lines obtain intensity via Auger cascade following the $2s$ photoionization. Since the double-ionization probability, studied for the $2p^5 3s^2$ states of atomic Al by Jänkälä *et al.* [3], decreases slowly within photon energies of 5 eV above threshold, the intensity is not increased owing to higher photo double-ionization cross section. Figure 4(b) shows the pure $L_{2,3}M$-MMM spectrum obtained as the difference between the two $L_{2,3}$-MM spectra shown in Fig. 3.

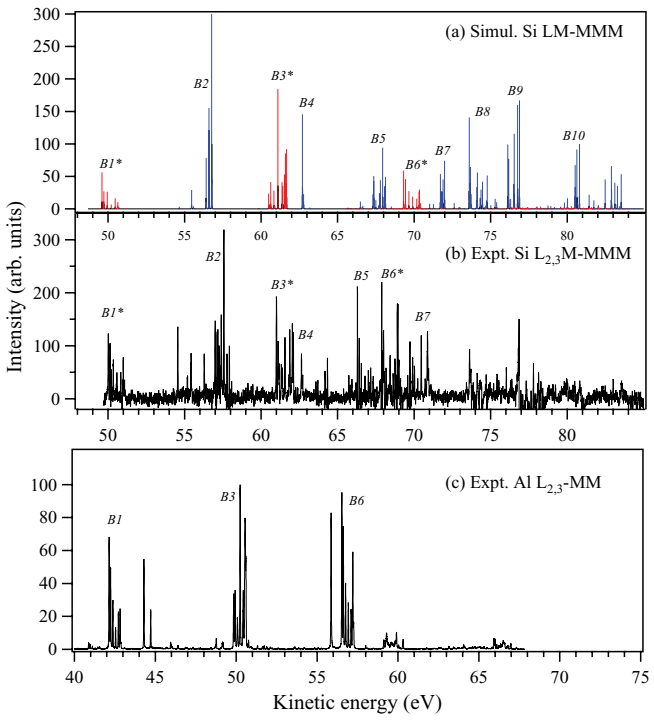

FIG. 4. (Color online) (a) Simulated and (b) experimental $L_{2,3}M$-MMM Auger spectrum of atomic Si. The simulated spectrum has been constructed with the MCDF calculations. The experimental Auger spectrum was obtained by subtracting the two spectra shown in figure 2 from each other. Labels for the transition groups from the even parity $2p$ ionized states are marked with asterisk. (c) Experimental $L_{2,3}$-MM Auger spectrum of atomic Al taken from Ref. [3].

The (second-step) $2p$ Auger spectrum consists of numerous narrow lines from several initial states. As shown previously for atomic Si and Al [3,4], the calculated $2p$ Auger spectrum is very sensitive to the configuration set used for the $2p$ hole states in the computations. The configuration set has to be enlarged to consist of several mixing configurations in order to achieve a decent correspondence between experimental and calculated kinetic energies and intensities for Al [3]. In this work, the final configuration set for the CK calculations was used as the configuration set for the $2p$ ionized states of Si. The Auger energies and transition rates from calculated initial states to the Si^{3+} $2p^6(3s,3p,3d)$ final states of a second Auger emission were computed. The intensities of the second-step Auger transitions were determined by redistribution of the population of the initial states obtained from the first-step calculations to the final states within the calculated Auger rates. The calculated Auger energies and intensities were used in simulation of the $L_{2,3}M$-MMM Auger spectrum displayed in Fig. 4(a). For this second step, the agreement between the simulated and measured spectra is fairly good when the total intensities of the various Auger groups are compared with each other. Within a given group, however, the individual intensities are not so well predicted. If the intensities of individual states are not correctly predicted during previous steps, the error accumulates in the final step of the Auger cascade. Nevertheless, the present computations enable us to assign detailed configurations to the Auger groups $B1$–$B7$ shown in Fig. 4(b). The assignments are given in Table II. Only the dominant electron configuration is given for the initial states. The $2p$-$3s$ coupled parent LS terms are also given if possible.

D. Comparison between Al and Si spectra

Normal photoionization of the $2p$ shell of the free Al atom creates isoelectronic states with the $2p$ ionized states of Si that are produced after the L_1-$L_{2,3}M$ CK transitions studied in this work. In the case of Al, the $2p$ ionized states were created by photoionization, which populates the $2p^5 3s^2 3p$ even-parity states. These photolines correspond to the Auger group $A1$ in Fig. 2. The Al $2p$ ionized states with odd parity are weak because they are produced via conjugated shake-up transitions with a rather small total relative probability of about 10%, among which the $3p \rightarrow 3d$ excitation dominates [3]. In contrast, in the case of silicon the $2p$ states of both parities, that is, those with a leading CSF from the $2p^5 3s^2 3p$ and $2p^5 3s 3p^2$ configurations, are populated via Auger cascade. The odd-parity states are predominantly populated with the experimental relative percentage of 82%.

In order to compare the Auger decay spectra of the isoelectronic $2p$ hole states, the $L_{2,3}M$-MMM spectrum of Si and the $L_{2,3}$-MM spectrum of Al are depicted in Figs. 4(b) and 4(c), respectively. The $L_{2,3}M$-MMM Auger lines of Si are shifted about 7 eV to higher kinetic energies as compared to Al. This is because of stronger electron-nucleus Coulomb attraction in Si in comparison to Al, resulting in larger splitting between ionic states in Si. The Auger groups $B1$, $B3$, and $B6$, originating from the $2p 3s^2 3p$ ionized states with even parity,

TABLE II. Assignments for Si $L_{2,3}M$-MMM Auger transition groups with initial and final configurations of transitions obtained by MCDF calculations. The parent LS terms are given in brackets for the initial states. Experimental kinetic energy (KE) regions (errors ±0.2 eV) and experimental and calculated relative intensities of $L_{2,3}M$-MMM Auger groups are also shown. The intensity ratios were obtained from the subtracted spectrum shown in Fig. 4(b).

				Relative intensity	
Label	Initial state	Final state	KE (eV)	Expt.	Theory
$B1$	$2p^5 3s^2 3p$	$2p^6 3d$	49.9–51.2	54	25
$B2$	$2p^5 3s(^1P)3p^2(^3P)$	$2p^6 3d$	54.5–58.1	151	138
$B3$	$2p^5 3s^2 3p$	$2p^6 3p$	60.9–62.2	100	100
$B4$	$2p^5 3s(^3P)3p^2(^3P)$	$2p^6 3d$	62.5–62.8	14	31
$B5$	$2p^5 3s(^1P)3p^2(^3P)$	$2p^6 3p$	65.6–66.6	24	61
$B6$	$2p^5 3s^2 3p$	$2p^6 3s$	67.7–69.3	77	36
$B7$	$2p^5 3s(^{1,3}P)3p^2(^1D)$	$2p^6 3p$	69.8–71.2	66	34
$B8$	$2p^5 3s(^3P)3p^2(^3P)$	$2p^6 3p$			81
$B9$	$2p^5 3s(^1P)3p^2(^3P)$	$2p^6 3s$			100
$B10$	$2p^5 3s 3p^2(^1D)$	$2p^6 3s$			44

are found in both the Si and Al spectra. We note two interesting features. First, the Auger groups $B1$, $B3$, and $B6$ look very similar in Si and Al spectra, which indicates that the initial state populations created by different processes are very similar in the current case. Secondly, the intensity ratios of the Auger groups $B1$, $B3$, and $B6$ are 19:40:41 for Al and 23:43:33 for Si. These values are independent of the initial-state populations. Thus, the difference is mainly explained by the difference in the final-state $3s$, $3p$, and $3d$ radial wave functions owing to different screenings of the nuclear potential. The calculations predict the group intensities of 13:48:39 for Al and 16:62:22 for Si, so in both cases the group intensities of $B1$ and $B6$ are underestimated and the group intensity of $B3$ is overestimated. However, the tendency of smaller relative intensity of the $B6$ group in Si is accounted for. The Auger groups $B2$, $B4$, $B5$, and $B7$–$B10$ appear only in the Si spectrum. These Auger states originate from the $2p$ ionized states with odd parity. Since these Auger groups have odd-parity electron configuration as an initial state, they do not have counterparts in the Al Auger spectrum.

The Auger matrix elements between the $2p$ ionized states and $2p^6 nl$ final states were studied in order to find the $2p$ ionized CSFs that contribute predominantly in the Auger groups $B1$–$B6$. It was found that the Auger transitions $B1$ take place owing to the $2p^5 3s^2 3p$-$2p^5 3s 3p 3d$ configuration interactions and the Auger transitions $B3$ owing to the $2p^5 3s^2 3p$-$2p^5 3p^3$ configuration interactions in the Si spectrum. The results are similar to those of the previous Al study [3]. For the odd-parity $2p$ ionized states, the configuration interaction between $2p^5 3s 3p^2$ and $2p^5 3p^2 3d$ was found to be crucial in predicting the Auger groups $B2$ and $B4$, as the Auger matrix elements between the $2p^5 3p^2 3d$ and $2p^6 3d$ CSFs are the most significant. In contrast, the electron correlation is not significant in predicting the Auger intensity of the groups $B5$ and $B6$, as the Auger matrix elements between the $2p^5 3s 3p^2$ and $2p^6 3p$ and $2p^5 3s^2 3p$ and $2p^6 3s$ CSFs are the largest.

V. CONCLUSIONS

The $2s$ photoelectron spectrum and subsequent Auger transition cascade consisting of the L_1-$L_{2,3}M$ CK and $L_{2,3}M$-MMM Auger transitions were measured at several photon energies and identified with the aid of MCDF calculations. The binding energies and natural linewidths of 1.2 eV for the $2s$ photolines were determined. The five lowest $2s 3s^2 3p^2$ states are mostly populated during the photoionization. These core-ionized states deexcite via the L_1-$L_{2,3}M$ CK transition, which populates both the even-parity $2s^2 2p^5 3s^2 3p$ and odd-parity $2s^2 2p^5 3s 3p^2$ states and their satellites. The $2p$ ionized intermediate states further decay by the second-step $L_{2,3}M$-MMM Auger transitions leading to the $2p^6 nl$ final states. In order to properly take into account the prominent electron correlation, a large configuration set was applied during the MCDF calculations of the Auger transition cascade. The $L_{2,3}M$-MMM Auger spectrum of Si was compared to the previously measured photon-induced $L_{2,3}$-MM spectrum of Al, which originates from the transitions between the isoelectronic configuration states. It was demonstrated that, because of the Auger cascade process, the $2p$ Auger spectrum of Si provides more information on intermediate ionic states than the corresponding $2p$ Auger spectrum of Al. In the Al case, the $2p$ ionized states with even parity were populated while in the Si case both the even- and odd-parity states were populated. The electron correlation was found to affect equally the even-parity $2p$ ionized states of Si and Al.

ACKNOWLEDGMENTS

The staff of MAX laboratory is acknowledged for assistance during the measurements. S.U. would like to acknowledge the Vilho, Kalle, and Yrjö Väisälä Foundation for financial support. This work has been financially supported by the Research Council for Natural Sciences and Technology of the Academy of Finland and by the European Community's ARI program.

[1] S. Fritzsche, K. Jänkälä, M. Huttula, S. Urpelainen, and H. Aksela, Phys. Rev. A **78**, 032514 (2008).

[2] M. Huttula, K. Jänkälä, A. Mäkinen, H. Aksela, and S. Aksela, New J. Phys. **10**, 013009 (2008).

[3] K. Jänkälä, S. Fritzsche, M. Huttula, J. Schulz, S. Urpelainen, S. Heinäsmäki, S. Aksela, and H. Aksela, J. Phys. B **40**, 3435 (2007).

[4] K. Jänkälä, S. Urpelainen, M. Huttula, S. Fritzsche, S. Heinäsmäki, S. Aksela, and H. Aksela, Phys. Rev. A **77**, 062504 (2008).

[5] M. Huttula, S. Heinäsmäki, H. Aksela, E. Kukk, and S. Aksela, J. Electron Spectrosc. Relat. Phenom. **156**, 270 (2007).

[6] I. P. Grant, *Relativistic Quantum Theory of Atoms and Molecules: Theory and Computation*, Springer Series on Atomic, Optical, and Plasma Physics, Vol. 40 (Springer, New York, 2007)

[7] F. A. Parpia, C. Froese Fischer, and I. P. Grant, Comput. Phys. Commun. **94**, 249 (1996).

[8] S. Fritzsche, J. Electron Spectrosc. Relat. Phenom. **114**, 1155 (2001).

[9] S. Fritzsche, H. Aksela, C. Z. Dong, S. Heinäsmäki, and J. E. Sienkiewicz, Nucl. Instrum. Methods Phys. Res. B **205**, 93 (2003).

[10] S. Fritzsche, J. Nikkinen, S.-M. Huttula, H. Aksela, M. Huttula, and S. Aksela, Phys. Rev. A **75**, 012501 (2007).

[11] G. Gaigalas, S. Fritzsche, and I. P. Grant, Comput. Phys. Commun. **139**, 263 (2001).

[12] G. Gaigalas, T. Zalandauskas, and S. Fritzsche, Comput. Phys. Commun. **157**, 239 (2004).

[13] J. Nikkinen, H. Aksela, S. Heinäsmäki, S. Fritzsche, E. Kukk, M. Huttula, and S. Aksela, Phys. Rev. A **66**, 064703 (2002).

[14] S. Fritzsche, B. Fricke, and W. D. Sepp, Phys. Rev. A **45**, 1465 (1992).

[15] Yu. Ralchenko, A. E. Kramida, J. Reader, and NIST ASD Team, NIST Atomic Spectra Database (version 3.1.5) [http://physics.nist.gov/asd3]. National Institute of Standards and Technology, Gaithersburg, MD.